

Large-gap quantum spin Hall state on a semiconductor surface:

The orbital filtering by substrate

Miao Zhou¹, Wenmei Ming¹, Zheng Liu¹, Zhengfei Wang¹, Yugui Yao², and Feng Liu^{1*}

¹ Department of Materials Science and Engineering, University of Utah, UT 84112

² School of Physics, Beijing Institute of Technology, Beijing, China 100081

**fliu@eng.utah.edu*

For potential applications in spintronics and quantum computing, it is desirable to place a quantum spin Hall insulator [i.e., a 2D topological insulator (TI)] on a substrate while maintaining a large energy gap. Here, we demonstrate an approach to create the large-gap 2D TI state on a semiconductor surface, based on first-principles calculations. We show that when Bi, Pb and Au atoms are deposited on a patterned H-Si(111) surface into a hexagonal lattice, both the Bi@H-Si(111) and Pb@H-Si(111) surfaces exhibit a 2D TI state with a large gap of ≥ 0.5 eV while the Au@H-Si(111) surface is a trivial insulator. These interesting results are found to originate from the fact that the H-Si(111) surface acts as an “atomic” orbital filter to critically select the orbital composition around the Fermi level, resulting in different topological phases. In particular, the substrate orbital filtering effect converts the otherwise topologically trivial freestanding Bi and Pb lattices into a nontrivial phase; while the reverse is true for the Au lattice. The physical mechanism underlying this approach is generally applicable, opening up a new and exciting avenue for future design and fabrication of large-gap topological surface/interface states.

Recently there has been a surge in the investigation of topological insulators (TIs) [1–3]. TIs are distinguished from conventional insulators by robust metallic surface or edge states residing inside an insulating bulk gap. As these topological states are protected by time reversal symmetry, they have negligible elastic scattering and Anderson localization [4, 5], rendering significant implications in electronic/spintronic and quantum computing devices. To realize their potential applications, it is desirable for the TIs to have an energy gap as large as possible [6]. As for 2D TIs [i.e., quantum spin Hall (QSH) insulators], they also need to be grown or placed onto a substrate [7-10] or formed as an interface [11, 12], while maintaining a large gap. So far, however, this goal remains allusive.

The HgTe quantum well, as the first theoretically predicted [11] and experimentally confirmed [12] QSH insulator, has a small gap of 40 meV with topological edge states only detectable at very low temperature (<10 K) [12]. Recent studies pertaining to Bi/Sb(111) films [13–16], Sn films [17], metal-decorated graphene [18-20], silicene/germanene [21] and 2D organometallic frameworks [22–25] have largely enriched the family of 2D TIs, and some of them have a large gap [13, 17, 20]. However, a critical drawback with most previous theoretical studies of 2D TIs is their reliance on the electronic and topological properties of freestanding films, whose existence can be in doubt. Even a freestanding film does exist, its properties are expected to be influenced by the underlying substrate in real applications [8-10]. Here, we demonstrate a unique approach of creating QSH state on a conventional semiconductor surface where the substrate plays a “positive” role acting as an orbital filter to critically select the orbital composition around the Fermi level, so that the nontrivial topological state arises with a large gap.

We have performed first-principles calculations of band structure and band topology of 2D

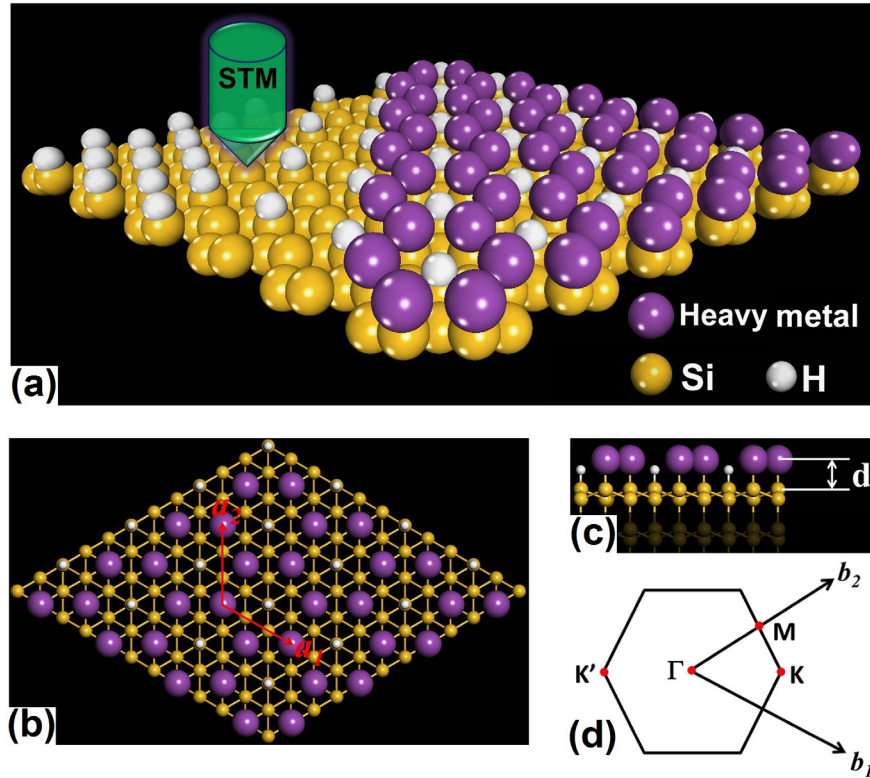


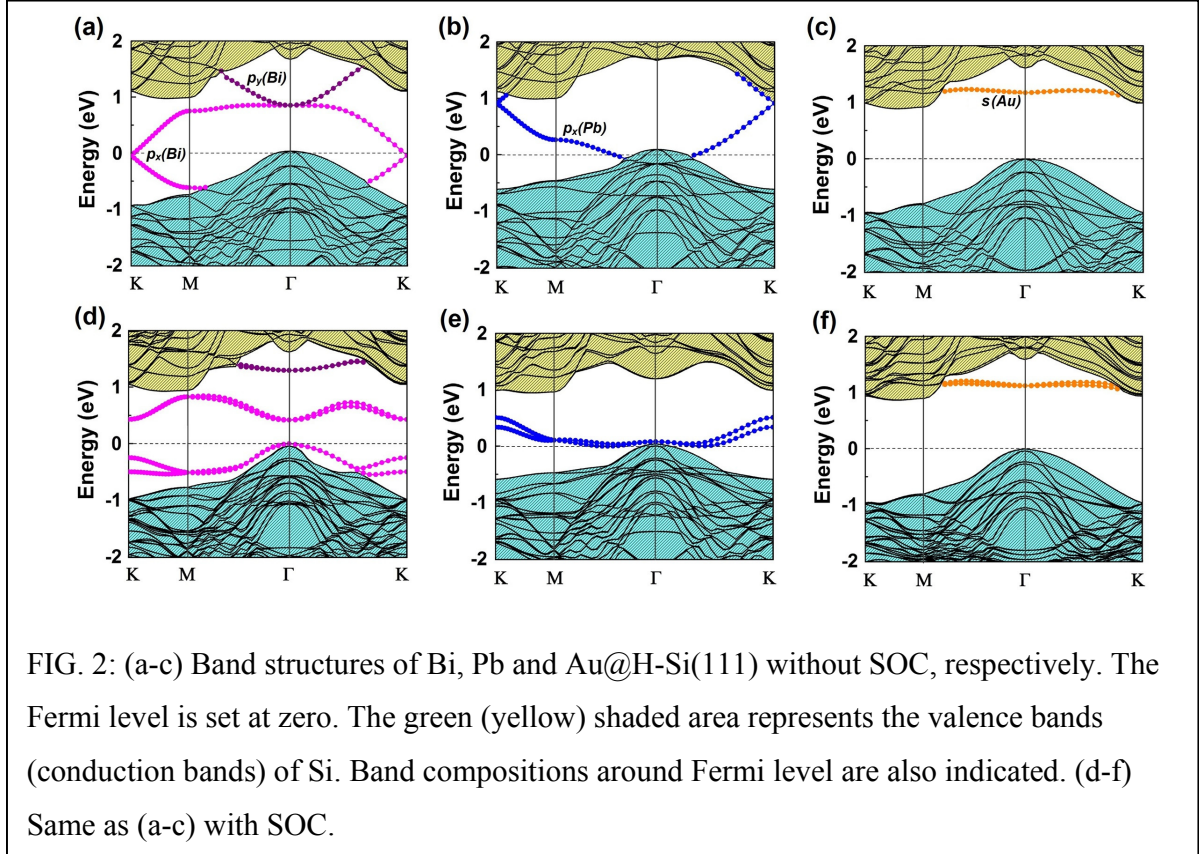
FIG. 1: (a) Schematic of a two-step approach to fabricate 2D TI by deposition of heavy metal atoms on a patterned H-Si(111) surface. (b, c) The top and side view of the proposed structure, with the surface unit cell vector (a_1 , a_2) indicated in (b) and the adsorption length d in (c). (d) The first surface Brillouin zone.

hexagonal lattices of various metal atoms, including Bi, Pb, Au, Sb, Sn, Ga, In and Tl, grown on a patterned H-saturated Si(111) surface. In the main text below, we will discuss in detail the results of Bi, Pb and Au, as representative examples, and leave the results of other metals in the Supplementary Information [26]. Atomically flat H-Si(111) surface has been prepared for decades and is a widely-used substrate for epitaxial growth of ordered overlayers [27, 28]. The surface dangling bonds are passivated by H to avoid surface reconstruction. In order to form a hexagonal metal overlayer lattice, we propose a two-step fabrication process, as shown in Fig. 1. First, to create a desirable surface template pattern for metal growth, H atoms are selectively

removed in hexagonal symmetry using scanning tunneling microscopy, as discussed in Refs. [29, 30]; Second, heavy metal atoms with large spin-orbit coupling (SOC) can be deposited to grow or self-assemble into the exposed Si sites, as already demonstrated for other systems [31-33].

We found a very strong binding between the deposited metal atoms and the exposed Si atoms in the H-Si(111) surface, as evidenced by the calculated adsorption length (d) of 2.68 Å, 2.75 Å and 2.30 Å for Bi, Pb and Au, respectively. The high structural stability is also indicated by a large adsorption energy (E_{ad}), defined as $E_{ad} = E_{M@H-Si(111)} - (2E_M + E_{H-Si(111)}) + E_{H_2}$, where $E_{M@H-Si(111)}$, E_M , $E_{H-Si(111)}$ and E_{H_2} denote the energy of Bi/Pb/Au@H-Si(111), single metal atom, pristine H-Si(111) surface and H₂ gas molecule, respectively. The adsorption energy is found to be 3.88 eV, 3.92 eV and 4.10 eV for Bi, Pb and Au, respectively, which are comparable to the binding energies of most elemental crystalline solids.

To examine the band topology of such surface structures, we first purposely exclude SOC from calculation. The resulting band structures for Bi, Pb and Au@H-Si(111) are shown in Figs. 2 (a-c), respectively. For Bi@H-Si(111), there are two Dirac bands residing inside the bulk gap of Si with a Dirac point at K point, which locates nearby the Fermi level (Fig. 4(a)). Analysis of band composition further showed that the two Dirac bands consist mainly of p_x orbitals of Bi atoms. Another dispersive band, consisting of p_y orbitals of Bi, sits below the bulk conduction band edge of Si and touches the upper Dirac band of p_x orbitals at Γ point. The band structure of Pb@H-Si(111) is similar to the case of Bi, represented by two Dirac bands inside the Si gap; but the Dirac point sits ~0.8 eV above Fermi level [Fig. 2(b)], because Pb has one less valence electron than Bi. In sharp contrast to Bi and Pb, the band structure of Au@H-Si(111) is very different [Fig. 2(c)]. There is no Dirac band or Dirac point; it is a typical semiconductor surface with a large band gap of ~0.9 eV. Its surface states, coming mainly from 6s orbital of



Au atoms, are above the bulk conduction band edge of Si.

Next, we include SOC, and the resulting band structures are shown in Figs. 2(d-f). Comparing Fig. 2(d) with 2(a), one sees that for Bi@H-Si(111), two Dirac bands are split apart; one large energy gap of ~ 0.7 eV opens at K point, and another gap of ~ 0.5 eV opens at Γ point, which is the global gap. The p_y and the upper p_x bands are also separated by SOC, with an indirect gap ~ 0.45 eV. We note that the spin degeneracy of these bands is lifted (most noticeable at K point), due to the Rashba effect [34] induced by the broken spatial inversion symmetry. Similarly, the SOC opens a gap at K point for Pb@H-Si(111), with the upper branch of Dirac bands moving completely into the Si conduction band, as shown in Fig. 4(e). Thus, an effective SOC gap of ~ 0.52 eV could be counted by the energy difference between the Si conduction band minimum and the top of the Pb p_x band. However, to truly make the Pb@H-Si(111) surface a 2D TI, n-type doping is needed to shift the Fermi level into the SOC gap. Again in sharp contrast to the case of

Bi and Pb, for Au@H-Si(111), the SOC causes little change in band structure [comparing Figs. 2(f) with (c)], except some Rashba-type of spin splitting.

The SOC-induced gap opening at the Dirac point in Bi@H-Si(111) and Pb@H-Si(111) indicates possible existence of 2D TI state. To check this, we calculated the topological edge states of Bi@H-Si(111) by the Wannier90 package [35]. Using DFT bands as input, we construct the maximally localized Wannier functions and fit a tight-binding Hamiltonian with these functions. Figure 3(a) shows the DFT and fitted band structures, which are in very good

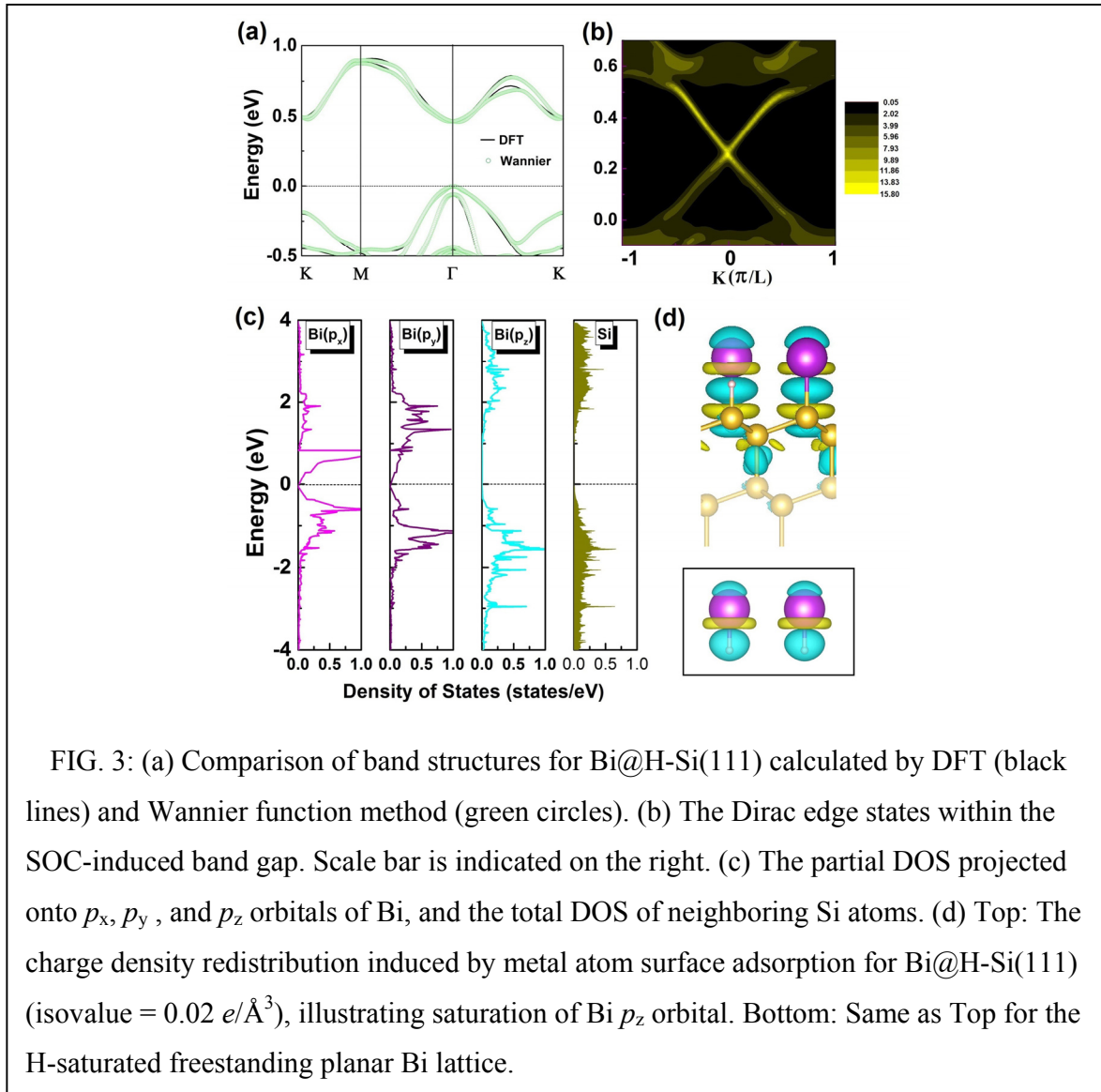


FIG. 3: (a) Comparison of band structures for Bi@H-Si(111) calculated by DFT (black lines) and Wannier function method (green circles). (b) The Dirac edge states within the SOC-induced band gap. Scale bar is indicated on the right. (c) The partial DOS projected onto p_x , p_y , and p_z orbitals of Bi, and the total DOS of neighboring Si atoms. (d) Top: The charge density redistribution induced by metal atom surface adsorption for Bi@H-Si(111) (isovalue = $0.02 e/\text{\AA}^3$), illustrating saturation of Bi p_z orbital. Bottom: Same as Top for the H-saturated freestanding planar Bi lattice.

agreement. Then, the edge Green's function of a semi-infinite Bi@H-Si(111) is constructed and the local density of state (DOS) of Bi zigzag edge is calculated, as shown in Fig. 3(b). Clearly, one sees gapless edge states that connect the upper and lower band edge of the bulk gap, forming a 1D Dirac cone at the center of Brillouin zone (Γ point). This indicates that the Bi@H-Si(111) is a 2D TI with a large gap of ~ 0.5 eV.

To further confirm the above topological edge-state results, we also calculated Z_2 topology number. As the spatial inversion symmetry is broken in these systems, we used the method developed by Xiao et al. [21, 36]. In this method, Z_2 is calculated by considering the Berry gauge potential and Berry curvature associated with the Bloch wave functions, which does not require any specific point-group symmetry. Indeed, we found that $Z_2 = 1$ for Bi@H-Si(111) (Fig. S1), confirming the existence of QSH state in this surface. Assuming a shift of Fermi level above the lower branch of Dirac band, we also found $Z_2 = 1$ for Pb@H-Si(111) (Fig. S2). In contrast, we found $Z_2 = 0$ for Au@H-Si(111) (Fig. S3).

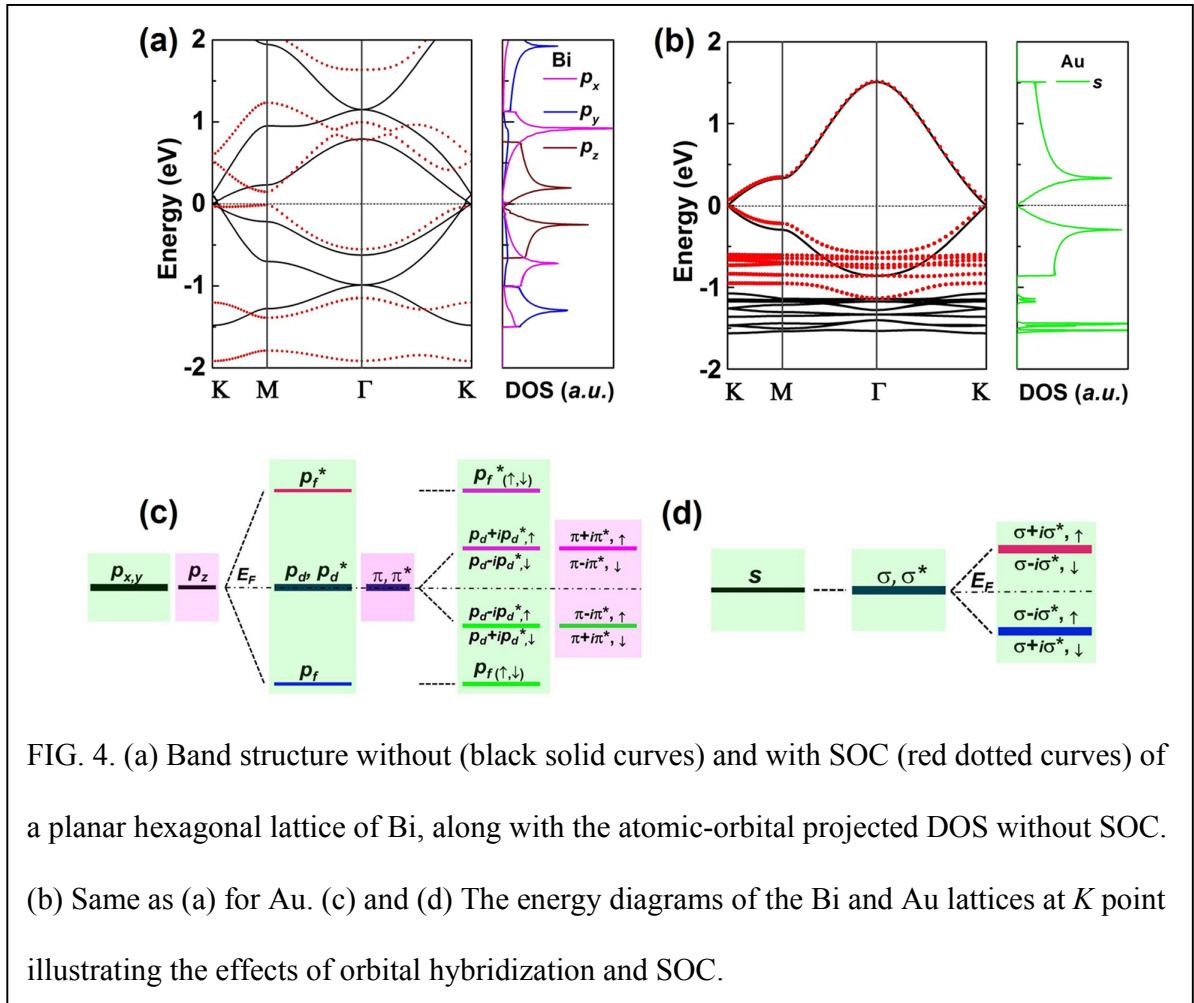
To understand the physical origin of QSH state in Bi@H-Si(111) or Pb@H-Si(111) but not in Au@H-Si(111), we next do an orbital analysis associated with the topological phase. Figure 3(c) shows the partial DOS of Bi@H-Si(111) around the Fermi level. It is seen that the p_z orbital of Bi hybridizes strongly with the dangling bond of the exposed surface Si atom overlapping in the same energy range [also seen from the charge density redistribution plotted in the upper panel of Fig. 3(d)]. It effectively removes the p_z bands away from the Fermi level, leaving only the p_x and p_y orbitals to form two Dirac bands and two flat bands, which can be described by a four-band model of topological phase in a hexagonal lattice [23, 37]. This indicates that the H-Si(111) substrate acts like an orbital filter, to selectively remove the p_z orbitals from the Bi lattice, reducing it from a trivial six-band lattice to a nontrivial four-band lattice, as we explain in the

following.

The concept of 2D TI was first proposed by the seminal work of Kane and Mele [18] using the graphene model, in which an energy gap is opened at Dirac point in proportion to the strength of SOC. Unfortunately, the SOC of graphene is negligibly small, and much effort has later been devoted to remedy this problem [19, 20]. There are two apparent key conditions in the Kane-Mele model to create a 2D TI. One is the lattice symmetry, such as the hexagonal symmetry that produces Dirac band; the other is the SOC. Given these two conditions alone, one might think to create a large-gap 2D TI by constructing a planar hexagonal lattice of heavy metal atoms with large SOC. However, this turned out not to be generally true because there is a third condition of “orbital selection” associated with the Kane-Mele model.

We have performed first-principles calculations of band structure and band topology of freestanding 2D planar hexagonal lattices of Bi and Au, to examine whether they are “theoretically” 2D TIs having a large energy gap. Figures 4(a) and (b) show the calculated band structures and DOS around Fermi level of Bi and Au, respectively. Surprisingly, the two lattices are found to have drastically different electronic and topological properties. The Bi lattice is a trivial insulator with $Z_2=0$, while the Au lattice is nontrivial with $Z_2=1$ (see Figs. S4-5). Their topological difference is found to originate from the different orbital composition around the Fermi level. For Bi, the valence bands consist of three (p_x , p_y , and p_z) orbitals [Figs. 4(a)]. The topology associated with the two bands from p_z orbital can be described by the single-orbital two-band Kane-Mele model; while the topology associated with other four bands from p_x and p_y orbitals can be described by the four-band model [23, 37]. Note that separately either the two-band or four-band model gives rise to nontrivial band topology ($Z_2=1$); however, counting all six bands together, the total band topology is trivial ($Z_2=0$), as two odd topological numbers

add to an even number (see Figs. S4-5). For Au, in contrast, the valence bands mainly consist of single s orbital, which form a Dirac point at K point without SOC, as shown in Fig. 2(b). The SOC opens a gap of ~ 70 meV, transforming the lattice into a 2D TI phase (Fig. S6). Thus, the Au lattice can also be understood by the Kane-Mele model, except that it involves a single s orbital rather than the p_z orbital in graphene.



More generally, we can better understand the topological phases in a 2D hexagonal lattice by a multi-orbital tight-binding model. The effective Hamiltonian with the nearest-neighbor hopping and intrinsic SOC can be written as,

$$\hat{H} = \sum_{i,l} \varepsilon_l c_{il}^\dagger c_{il} - \sum_{\langle i,j \rangle, l, l'} (t_{ijll'} c_{il}^\dagger c_{jl'} + H.c.) + \lambda_{SO} \hat{L} \cdot \hat{\sigma}, \quad (1)$$

where c_{il}^\dagger creates an electron of l -th orbital ($s, p_x, p_y, p_z, d_{xy}, \dots$) at site i . ε_l ($t_{ijll'}$) denotes the on-site energy (hopping energy) and λ_{SO} is the strength of SOC. As mentioned above, the Bi lattice can be described by the p -orbital six-band model, as illustrated in Fig. 4(c). Due to the planar symmetry, p_x and p_y orbitals hybridize to be distinguished from the p_z orbital, resulting in two branches of energy bands. The p_z branch of π and π^* bands is exactly the same as graphene [18]. The (p_x, p_y) branch has four bands: two flat bands (p_f, p_f^*) bracketing two dispersive bands (p_d, p_d^*) which form a Dirac point at K point. The SOC opens a gap in the dispersive bands at K point and mixes the p_d and p_d^* bands into two sets of $p_d \pm i p_d^*$ bands encoding a nontrivial topology. Again, the two branches of bands are both topologically nontrivial, but their sum becomes trivial. The Au lattice can be described by the s -orbital two-band model, as illustrated in Fig. 4(d). Without SOC, the two s orbitals hybridize into linearly dispersive two-fold degenerate σ and σ^* bands which touches at K point (Dirac point); the SOC opens a gap and mixes the σ and σ^* bands into two sets of $\sigma \pm i \sigma^*$ bands encoding a nontrivial topology.

There are two ways to make the planar hexagonal Bi lattice topologically nontrivial. The first way is by the well-known band inversion approach [11], which in the present case can be achieved by buckling the lattice into a non-planar structure [Fig. 5(a)], i.e., the single Bi(111) bilayer [13-15] as shown before. Figure 5(b) shows the band structure and DOS of a Bi(111) bilayer, which is confirmed with nontrivial topology [15]. In such a buckled structure, the Bi-Bi bond angle is around 90° , indicating that three (p_x, p_y and p_z) orbitals are degenerate with each other. Chemical bonding and crystal field splitting lifts the degeneracy and form one set of doubly degenerate $\sigma_{1,2}$ and $\sigma_{1,2}^*$ bands and another set of non-degenerate σ_3 and σ_3^* bands, in the

order of energy as shown in Fig. 5(c). The SOC opens an energy gap and further lifts the degeneracy of $\sigma_{1,2}$ and $\sigma_{1,2}^*$ bands, as well as causes a band inversion of energy order between $\sigma_{1\pm i2}$ and σ_3^* bands around the Fermi level. Consequently, the overall band topology becomes nontrivial.

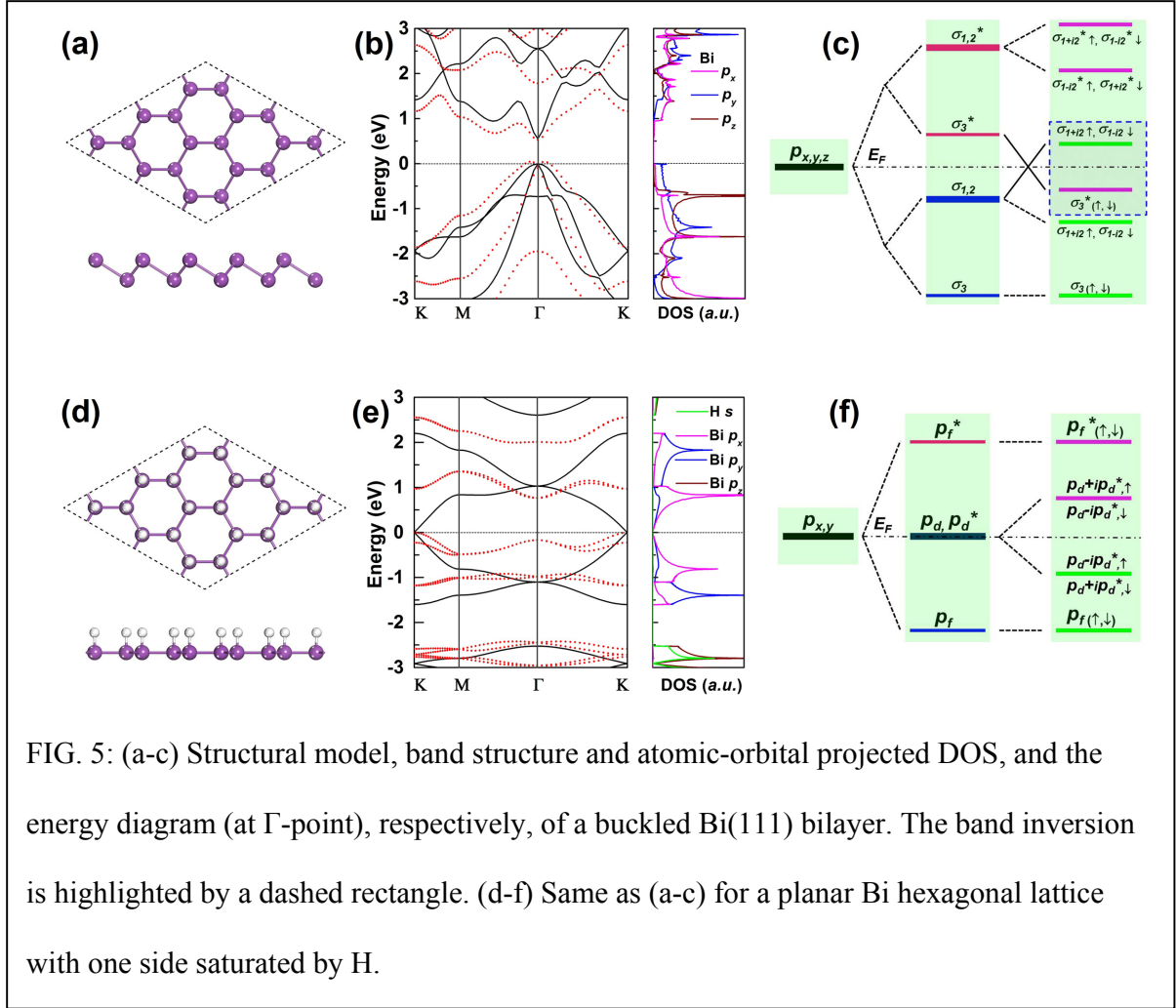


FIG. 5: (a-c) Structural model, band structure and atomic-orbital projected DOS, and the energy diagram (at Γ -point), respectively, of a buckled Bi(111) bilayer. The band inversion is highlighted by a dashed rectangle. (d-f) Same as (a-c) for a planar Bi hexagonal lattice with one side saturated by H.

The second approach is to simply remove one branch of orbitals [either (p_x, p_y) or p_z] to reduce the trivial six-band lattice into a nontrivial two- or four-band lattice. To verify this idea, we artificially saturate the planar hexagonal Bi lattice with H to remove the p_z orbital [Fig. 5(d)]. It is found that the p_z orbital of Bi hybridizes strongly with s orbital of H, shifting away from the

Fermi level, so that the system reduces to a (p_x, p_y) -orbital four-band model, which supports a nontrivial topological phase [Figs. 5(e) and (f)]. This is essentially what happens with the Bi@H-Si(111), where the exposed Si atom in the H-Si(111) surface fulfills the role of H atom to remove the p_z orbital of Bi, as shown in Fig. 3(d). In contrast, the Au atom has single s -orbital valence similar to H atom. When it is bonded with the exposed surface Si atom, it simply saturates the Si dangling bond just like the H does. Consequently, the band structure of Au@H-Si(111) is essentially the same as that of the semiconducting pristine H-Si(111) surface. Meantime, the Au-Si bond saturates the Au s -orbital and effectively removes the two s -orbital Dirac bands associated with the freestanding Au lattice, and hence its topological state [Figs. 1(c) and (f)].

Specifically, we can describe the Bi@H-Si(111) using a simplified (p_x, p_y) four-band model Hamiltonian in a hexagonal lattice as [23,37],

$$\hat{H}_{eff} = \begin{pmatrix} \varepsilon_0 & 0 & S_{xx} & S_{xy} \\ 0 & \varepsilon_0 & S_{xy} & S_{yy} \\ S_{xx}^* & S_{xy}^* & \varepsilon_0 & 0 \\ S_{xy}^* & S_{yy}^* & 0 & \varepsilon_0 \end{pmatrix} + \sigma_z \lambda_{so} \begin{pmatrix} 0 & -i & 0 & 0 \\ i & 0 & 0 & 0 \\ 0 & 0 & 0 & -i \\ 0 & 0 & i & 0 \end{pmatrix}, \quad (2)$$

in which $S_{xx} = V_{pp\sigma} + \left(\frac{1}{4}V_{pp\sigma} + \frac{3}{4}V_{pp\pi}\right) * (e^{ika_1} + e^{ik(a_1+a_2)})$, $S_{xy} = \frac{3}{4}(V_{pp\sigma} + V_{pp\pi}) * (e^{ika_1} + e^{ik(a_1+a_2)})$,

$S_{yy} = V_{pp\pi} + \left(\frac{3}{4}V_{pp\sigma} + \frac{1}{4}V_{pp\pi}\right) * (e^{ika_1} + e^{ik(a_1+a_2)})$, a_1, a_2 is the lattice vector, $V_{pp\sigma}$ ($V_{pp\pi}$) is the

Slater-Koster parameter [38], and $\sigma_z = \pm 1$ is the spin eigenvalue. This Hamiltonian produces either a flat-band Chern insulator [23], or a 2D TI, depending on the location of the Fermi level.

It is very intriguing to see that a topological trivial planar hexagonal Bi lattice becomes nontrivial when it is placed onto the H-Si(111) surface; while the reverse is true for the Au lattice, which is nontrivial by itself but becomes trivial on the H-Si(111) surface. This difference arises

from the very different orbital selection process in the two cases mediated by the metal adsorbate-substrate interaction, as discussed above. One subtle point is noted by comparing Bi@H-Si(111) and Pb@H-Si(111). The global gap is located at Γ point for Bi@H-Si(111) [Fig. 2(d)], but at K point for Pb@H-Si(111) [Fig. 2(e)]. This can be understood by analyzing the results of the four-band model [Eq. (2)] as a function of SOC strength, as shown in Fig. S7. With a small SOC, one gap (ΔE_1) opens at the Dirac point, and additionally two gaps (ΔE_2) open between the two flat and the upper and lower Dirac bands, respectively, at Γ point. With the increasing SOC strength, both ΔE_1 and ΔE_2 increase, which eventually leads to the formation of a different energy gap (ΔE_3) between the upper and lower Dirac bands at Γ point when ΔE_3 becomes smaller than both ΔE_1 and ΔE_2 . As such, for sufficiently large SOC, ΔE_3 replaces ΔE_1 to be the global gap, and correspondingly the global gap shifts from K to Γ point. This explains why the global gap is at K point for Pb@H-Si(111) but at Γ point for Bi@H-Si(111), because the SOC strength in p orbital of Pb (~ 0.91 eV) is smaller than that of Bi (~ 1.25 eV) [39].

Another interesting point resulting from the above comparison and analysis is that for the two-band model, the SOC gap increases linearly with the SOC strength [18]. But this is not true for the four-band model, only initially the SOC gap at the Fermi level increases with the increasing SOC; after the global gap shifts from K point to Γ point at a certain SOC as shown above, the SOC gap will start to decrease with the increasing SOC. This means that it is not necessarily true to have a large gap with a heavy atom of larger SOC, a noteworthy point for future design of TIs.

Besides Bi, Pb and Au, we have also done calculations of Sb, Sn, Tl, In and Ga. They all have similar band structures to Bi or Pb, except a different location of Fermi level due to different number of valence electrons (see Figs. S8-9). We point out that the importance of orbital

selection around the Fermi level has been discussed previously for both 2D and 3D TIs. Taking a few examples, for 2D TIs, the pristine Sn film belongs to the single-orbital (p_z) two-band Kane-Mele model; while the fluorinated Sn film is characterized by a six-band model (s , p_x and p_y orbitals) with band inversion [17]. The 2D hexagonal organometallic lattices can be classified into either a two-band (triphenyl-Bi, Pb) or four-band model (triphenyl-In) [22, 23]. For 3D TIs, the strained HgTe is characterized by a six-band model with band inversion between $|s, j=1/2\rangle$ and $|p, j=3/2\rangle$ states [11, 40]; while the BaBiO₃ is characterized by a four-band model with band inversion between $|s, j=1/2\rangle$ and $|p, j=1/2\rangle$ [41]. Another example is the Bi square “net” in SrMnBi₂ and CaMnBi₂, which belongs to a Bi (p_x, p_y) four-band model on a checkerboard lattice, with the Bi p_z orbital removed by interacting with neighboring Sr (Ca) layers [42, 43]. The orbital selection in TIs can also involve d orbitals [44, 45]. However, in all the previous examples, the orbital selection is a “natural” process, inherent to a given material. Here, we demonstrate the possibility of “controlled” manipulating the orbital selection by a unique approach of substrate orbital filtering process. Its underlying physical principle is general, applicable to deposition of different metal atoms on different substrates, which opens up a new and exciting avenue for future design and fabrication of large-gap topological surface/interface states.

Methods

Our electronic structure calculations based on density functional theory were performed by using a plane wave basis set [46] and the projector-augmented wave method [47], as implemented in the VASP code [48]. The exchange-correlation functional was treated with the generalized gradient approximation in Perdew-Burke-Ernzerhof format [49]. Calculations of Z_2 triviality were carried out by using the full-potential linearized augmented plane-wave method

implemented in the WIEN2K package [50]. Details for models and computations are presented in Supplementary Information [26].

References

- [1] Moore, J. E. The birth of topological insulators. *Nature* 464, 194-198 (2010).
- [2] Hasan, M. Z. & Kane, C. L. Colloquium: topological insulators. *Rev. Mod. Phys.* 82, 3045-3067 (2010).
- [3] Qi, X.-L. & Zhang, S.-C. Topological insulators and superconductors. *Rev. Mod. Phys.* 83, 1057-1110 (2011).
- [4] Bernevig, B. A. & Zhang, S.-C. Quantum spin hall effect. *Phys. Rev. Lett.* 96, 106802 (2006).
- [5] Xu, C. & Moore, J. E. Stability of the quantum spin Hall effect: Effects of interactions, disorder, and Z_2 topology. *Phys. Rev. B* 73, 045322 (2006).
- [6] Xia, Y. *et al.* Observation of a large-gap topological-insulator class with a single Dirac cone on the surface. *Nat. Phys.* 5, 398-402 (2009).
- [7] Yang, F. *et al.* Spatial and energy distribution of topological edge states in single Bi(111) bilayer. *Phys. Rev. Lett.* 109, 016801 (2012).
- [8] Hirahara, T. *et al.* Atomic and electronic structure of ultrathin Bi(111) films grown on Bi₂Te₃(111) substrate: Evidence for a strain-induced topological phase transition. *Phys. Rev. Lett.* 109, 227401 (2012).
- [9] Miao, L. *et al.* Quasiparticle dynamics in reshaped helical Dirac cone of topological insulators. *PNAS* 110, 2758 (2013).
- [10] Wang, Z. F. *et al.* Creation of helical Dirac fermions by interfacing two gapped systems of ordinary fermions. *Nat. Comm.* 4, 1384 (2013).

- [11] König, M. *et al.* Quantum spin Hall insulator state in HgTe quantum wells. *Science* 318, 766-770 (2007).
- [12] Chen, Y. L. *et al.* Experimental realization of a three-dimensional topological insulator, Bi₂Te₃. *Science* 325, 178-181 (2009).
- [13] Murakami, S. Quantum spin Hall effect and enhanced magnetic response by spin-orbit coupling. *Phys. Rev. Lett.* 97, 236805 (2006).
- [14] Wada, M. *et al.* Localized edge states in two-dimensional topological insulators: Ultrathin Bi films. *Phys. Rev. B* 83, 121310 (2011).
- [15] Liu, Z. *et al.* Stable nontrivial Z_2 topology in ultrathin Bi (111) films: a first-principles study. *Phys. Rev. Lett.* 107, 136805 (2011).
- [16] Zhang, P. F. *et al.* Topological and electronic transitions in a Sb(111) nanofilm: The interplay between quantum confinement and surface effect. *Phys. Rev. B* 85, 201410 (2012).
- [17] Xu, Y. *et al.* Large-gap quantum spin Hall insulators in Tin Films. *Phys. Rev. Lett.* 111, 136804 (2013).
- [18] Kane, C. L. & Mele, E. J. Quantum spin Hall effect in graphene. *Phys. Rev. Lett.* 95, 226801 (2005).
- [19] Weeks, C. *et al.* Engineering a robust quantum spin Hall state in graphene via adatom deposition. *Phys. Rev. X* 1, 021001 (2011).
- [20] Hu, J. *et al.* Giant topological insulator gap in graphene with 5d adatoms. *Phys. Rev. Lett.* 109, 266801 (2012).
- [21] Liu, C. C. *et al.* Quantum spin Hall effect in silicene and two-dimensional germanium. *Phys. Rev. Lett.* 107, 076802 (2011).

- [22] Wang, Z. F. *et al.* Organic topological insulators in organometallic lattices. *Nat. Comm.* 4, 1471 (2013).
- [23] Liu, Z. *et al.* Flat Chern Band in a Two-Dimensional Organometallic Framework. *Phys. Rev. Lett.* 110, 106804 (2013).
- [24] Wang, Z. F. *et al.* Prediction of a Two-Dimensional Organic Topological. *Nano Lett.* 13, 2842 (2013).
- [25] Wang, Z. F. *et al.* Quantum anomalous Hall effect in 2D organic topological insulator. *Phys. Rev. Lett.* 110, 196801 (2013).
- [26] See Supplementary Information for computational details, Z_2 invariant calculation results, tight-binding model, and band structures of Sb, Sn, Ga, In and Tl@H-Si(111).
- [27] Higashi, G. S. *et al.* Ideal hydrogen termination of the Si-(111) surface *Appl. Phys. Lett.* 56, 656-658 (1990).
- [28] Tada, H. *et al.* Epitaxial growth of vanadyl-phthalocyanine ultrathin films on hydrogen-terminated Si(111) surfaces. *Appl. Phys. Lett.* 61, 2021-2023 (1992).
- [29] Shen, T.-C. *et al.* Atomic-scale desorption through electronic and vibrational excitation mechanisms. *Science* 268, 1590-1592 (1995).
- [30] Schofield, S. R. *et al.* Quantum engineering at the silicon surface using dangling bonds. *Nat. Comm.* 4, 1649 (2013).
- [31] Gomes, K. K. *et al.* Designer Dirac fermions and topological phases in molecular graphene. *Nature* 483, 306-310 (2012).
- [32] Polini, M. *et al.* Artificial honeycomb lattices for electrons, atoms and photons. *Nat. Nanotechnol.* 8, 625-633 (2013).

- [33] Michalak, D. J. *et al.* Nanopatterning Si(111) surfaces as a selective surface-chemistry route. *Nat. Mater.* 9, 266-271 (2010).
- [34] Bychkov Y. A. & Rashba, E. I. Properties of a 2D electron gas with lifted spectral degeneracy. *JETP Lett.* 39, 78 (1984).
- [35] Mostofi, A. A. *et al.* Wannier90: a tool for obtaining maximally-localized wannier functions. *Comput. Phys. Commun.* 178, 685-699 (2008).
- [36] Xiao, D. *et al.* Half-Heusler compounds as a new class of three-dimensional topological insulators. *Phys. Rev. Lett.* 105, 096404 (2010).
- [37] Wu, C. & Das Sarma, S. $p_{x,y}$ -orbital counterpart of graphene: Cold atoms in the honeycomb optical lattice. *Phys. Rev B* 77, 235107 (2008).
- [38] Slater, J. C. & Koster, G. F. Simplified LCAO method for the periodic potential problem. *Phys. Rev.* 94. 1498-1524 (1954).
- [39] Bian, G. *et al.* Origin of giant Rashba spin splitting in Bi/Ag surface alloys. *Phys. Rev B* 88, 085427 (2013).
- [40] Brüne, C. *et al.* Quantum Hall effect from the topological surface states of strained bulk HgTe. *Phys. Rev. Lett.* 106, 126803 (2011).
- [41] Yan, B. *et al.* A large-energy-gap oxide topological insulator based on the superconductor BaBiO₃. *Nat. Phys.* 9, 709-711 (2013).
- [42] Park, J. *et al.* Anisotropic Dirac fermions in a Bi square net of SrMnBi₂. *Phys. Rev. Lett.* 107, 126402 (2011).
- [43] Lee, G. *et al.* Anisotropic Dirac electronic structures of AMnBi₂ ($A = \text{Sr, Ca}$) *Phys. Rev. B* 87, 245104 (2013).

[44] Xiao, D. *et al.* Interface engineering of quantum Hall effects in digital transition metal oxide heterostructures. *Nat. Comm.* 2, 596 (2011).

[45] Cai, T. Y. *et al.* Emergent topological and half semimetallic Dirac Fermions at oxide interfaces. *arXiv:1310.2471*.

[46] Blöchl, P. E. Projector augmented-wave method. *Phys. Rev. B* 50, 17953 (1994).

[47] Kresse, G. & Joubert, D. From ultrasoft pseudopotentials to the projector augmented-wave method. *Phys. Rev. B* 59, 1758 (1999).

[48] Kresse G. & Hafner, J. *Ab initio* molecular dynamics for liquid metals. *Phys. Rev. B* 47, 558 (1993).

[49] Perdew, J. P. *et al.* Generalized Gradient Approximation Made Simple. *Phys. Rev. Lett.* 77, 3865 (1996).

[50] Blaha, P. *et al.* WIEN2K: An Augmented Plane Wave and Local Orbitals Program for Calculating Crystal Properties (Vienna University of Technology, Vienna, Austria, 2001).

Acknowledgements

This research was supported by DOE (Grant No: DEFG02-04ER46148); Z. F. Wang and W. Ming additionally thank support from NSF-MRSEC (Grant No. DMR-1121252). We thank NERSC and the CHPC at University of Utah for providing the computing resources.

Author contributions

M. Z. carried out the theoretical calculations with the assistance of W. M. M., Z. L., Z. F. W. and Y. G. Y.; F. L. guided the overall project. M. Z. and F. L. wrote the manuscript.

Additional information

Supplementary Information accompanies this paper is available.

Competing financial interests: The authors declare no competing financial interests.